# Flexibility of the α-Spectrin N-Terminus by EPR and Fluorescence Polarization

L. Cherry, L. W.-M. Fung, and N. Menhart
Department of Chemistry, Loyola University of Chicago, Chicago, Illinois 60626 USA

ABSTRACT The structure and flexibility of the biologically important α-spectrin amino terminal region was examined by the use of fluorescence and EPR spectroscopy. The region studied has been previously demonstrated to be essential for the α-spectrin:β-spectrin association of the tetramerization site. Appropriate spectroscopic probe moieties were coupled to this region in a recombinant fragment of human erythroid α-spectrin. There was good agreement between the EPR and fluorescence techniques in most of this region. Mobility determinations indicated that a portion of the region was relatively immobilized. This is significant, since although predictive methods have indicated that this region should be α-helical, previous experimental evidence obtained on smaller synthetic peptides had indicated that this region was disordered. Observed rigidity appears to be incompatible with such a disordered state, and has important ramifications for the flexibility of this molecule that is so integral to its role in stabilizing erythrocyte membranes.

## INTRODUCTION

Spectrin is a protein underlying the surface of the erythrocyte lipid bilayer. Through its association with various integral membrane proteins, it is thought to be largely responsible for this membrane's flexibility and deformability, which allows red cells to survive physical stress during circulation through the vascular system (Agre, 1992). Spectrin is composed of two subunits, α-spectrin and β-spectrin, which associate laterally to form αβ heterodimers (Speicher et al., 1982; Shotton et al., 1979). These then further associate in an end-to-end fashion to form the biologically significant $(\alpha\beta)_2$ tetramer (Byers and Branton, 1985; Liu et al., 1987; Vertessy and Steck, 1989). Impaired tetramer formation leads to a large set of disorders called hereditary anemias in which erythrocytes exhibit unusually high fragility.

α-Spectrin and β-spectrin both consist largely of tandemly aligned repeat units of approximately 106 amino acids (Speicher et al., 1983a,b; Sahr et al., 1990; Winkelmann et al., 1990). α-Spectrin contains 22 of these repeat units and β-spectrin contains 18. These are thought to fold into compact triple α-helical structures, based on x-ray and NMR studies of homologous recombinant spectrin fragments (Yan et al., 1993; Pascual et al., 1997; Grum et al., 1999). In this model, each motif is composed of three approximately 30-residue helices arranged with the first and third helices parallel and the second intervening helix antiparallel. This zigzag arrangement places the amino and carboxyl ends of this domain on opposite ends of this structure, so that tandem alignment of these motifs creates a long rod-like molecule for both α and β spectrin. These then associate laterally to form a thicker, but still rod-like, αβ dimer (Speicher et al., 1992).

Formation of the physiologically relevant $(\alpha\beta)_2$ tetramer then proceeds by head-to-head association to form a longer rod. This is predicated on interactions between the ends of each of these αβ dimer rods that contain the N-terminus of α-spectrin and the C-terminus of β-spectrin (Morris and Ralston, 1989; DeSilva et al., 1992; Speicher et al., 1993). Two such symmetrical interactions are thus thought to occur, each between the N-terminus of α-spectrin in one dimer and the C-terminus of β-spectrin in the other dimer. These regions can be seen by sequence homology to contain fractional 106-amino acid repeat motifs. When these fractional motifs are examined in relation to the structural model, the β-subunit fractional motif appears to correspond to the first two helices of the three helix bundle and that of the α-subunit to the third helix. During tetramer formation, these fractional motifs are thought come together to form a heteropolypeptide three-helix bundle very similar to the normal bundles composed of a single polypeptide. The majority of spectrin mutations resulting in hereditary anemias and impaired dimer-dimer association occur in these regions (Marchesi, 1989; Eber et al., 1988; McGuire and Agre, 1988; Gallagher et al., 1991; Palek and Lambert, 1990).

We have previously shown that deletion of a small region before this fractional motif at the N-terminus of α-spectrin does not significantly affect association of a recombinant α-spectrin peptide with the β-monomer. However, further deletions into this fractional motif completely abolish association ($IC_{50}$ diminished by more than 2 orders of magnitude; Cherry et al., 1999). This recombinant work corroborates previous studies (Speicher et al., 1993) that showed that proteolysis of this region to remove portions of the fractional motif also disrupts α:β binding. The major region for tetramer formation is, therefore, located in this fractional motif region.

*Received for publication 6 December 1999 and in final form 11 April 2000.*

Dr. Cherry's current address: Department of Rheumatology, Immunology and Allergy, Brigham and Women's Hospital, Boston, MA 02115. E-mail: lcherry@rics.bwh.harvard.edu.

Address reprint requests to N. Menhart, Department of Chemistry, Loyola University of Chicago, 6525 N. Sheridan Rd., Chicago, IL 60626. E-mail: nmenhar@luc.edu.



0006-3495/00/07/526/10 $2.00

However, two factors illuminated in our binding study lead us to conclude that this interaction was not the sole factor driving the tetramerization reaction: an unusually large temperature dependence, and an undetectable dependence on ionic strength. Conversely, the spectrin tetramerization reaction is strongly ionic strength dependent, but has a lower temperature variation (Morris and Ralston, 1994; Morris and Ralston, 1989; Begg et al., 1997). This led us to propose that other factors may be involved in the tetramerization reaction (see Fig. 1 in Cherry et al., 1999). An interesting possibility was provided by previous observations that small synthetic peptide homologues of the α-spectrin amino terminal region are disordered (i.e., not helical) and do not interact with β-spectrin. Could it be that helical unwinding of the separated fractional motifs is responsible for the observed differences? Recent work has demonstrated that α-helices can exist in equilibrium with their disordered states, and that the extent of disorder varies at different positions within the helix (Venyaminov et al., 1999; Holtzer et al., 1997; d'Avignon et al., 1998). It has also been shown by NMR that portions of intact spectrin can become highly disordered under some circumstances (Begg et al., 1994); however, it was impossible to determine which regions these were due to the large size of spectrin.

As such, we used paramagnetic and fluorescent probes to gain information about local order along this fractional motif, in the context of a larger recombinant α-spectrin fragment. This fragment has been shown have similar stability and binding properties compared to intact α-spectrin. Because disordered structure is expected to be highly flexible and mobile, probes attached to disordered regions are expected to exhibit rapid motion and helical regions (or other types of defined structures) less rapid motion. The use of two types of probes, and thus two independent types of measurement protocols, allows us to corroborate our results and increase the confidence in our conclusions. We found that most of the amino terminal region exhibits restricted motion inconsistent with disordered structure.

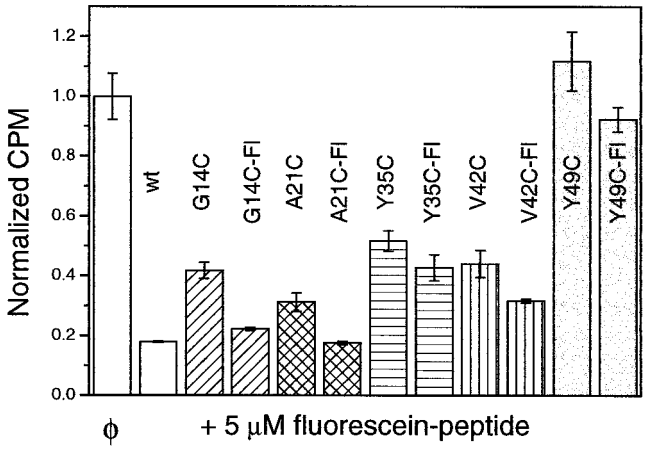


FIGURE 1 Binding of labeled Cys variant peptides with β-spectrin. Coupling of a probe moiety (fluorescein) was also shown to not reduce binding by single point displacement reactions in which 5 μM fluorescein-labeled or unlabeled variant protein was used to displace radiolabeled α-spectrin peptides from immobilized β-spectrin. In all cases the conjugation of fluorescein did not interfere with β-spectrin binding. That is, in all cases, the labeled protein displaced at least as much bound radioactivity as the unlabeled probe. This indicates that the labeled proteins have $IC_{50}$ values at least as low as the unlabeled protein (given in Table 1), which are very similar to the wild-type value. The 28Cys variant is not shown since this is a known mutation and had been determined to cause defective β-spectrin binding. The 49Cys variant also appears to abolish binding, which again is not unexpected, since although the specific Cys substitution is not known, other substitutions at this position are known to impair spectrin association.

## MATERIALS AND METHODS

### Recombinant α-spectrin fragments

Our methods for recombinant spectrin peptide production have been published (Menhart et al., 1996; Lusitani et al., 1998; Cherry et al., 1999). The particular peptide we are concerned with herein consists of the first 368 residues of α-spectrin. We made variants of this parent peptide by first mutating the endogenous Cys residues to Ala (at 167, 224, and 325), and then reintroducing individual Cys residues in the amino terminal region at positions 14, 21, 28, 35, 42, and 49. This seven-residue periodicity was chosen to minimize differences between the peptides should the region indeed assume an α-helix, since in that case all positions would lie along one face.

### Spin-labeling and fluorescent labeling of α-Sp peptides

α-Spectrin peptides were labeled as described (Cherry, 1999). Briefly, ~0.5 mg was concentrated to 10 mg/ml, and 2 mg of dithiothreitol was added with incubation for 1 h at 37°C. Following desalting by gel filtration in 5 mM Na phosphate pH 7.4 150 mM NaCl (PBS), 10-fold molar excess of the methanethiosulfonate spin-label (MTSSL; Toronto Research Chemicals, Toronto, ON) or 10-fold excess 5-iodoacetamido-fluorescein (Molecular Probes, Eugene, OR) was added and incubation continued for 1 h and 3–5 h, respectively, at room temperature in the dark. Excess probe was again removed by gel filtration. The ratio of probe to peptide was determined spectroscopically against 4-hydroxy TEMPO standards (EPR) or by absorption (fluorescence).

### Peptide characterization

We measured the overall helicity of the peptides by circular dichroism, as previously described (Menhart et al., 1996). Biological functionality of the peptides was ascertained by a microtiter plate binding assay toward intact β-spectrin (Cherry et al., 1999). Briefly, various concentrations of unlabeled test peptide (each of the variants) were used to displace a small but constant amount of $^{125}$I-labeled wild-type peptide from β-spectrin immobilized on microtiter plates. By varying the concentration of the test peptide, a titration curve could be produced, and the $IC_{50}$ could be determined. Additionally, in order to determine if conjugation of the probe moiety interfered with this binding, single point displacement assays in which 5 μM unlabeled or fluorescein-conjugated Cys variant peptides were used to displace labeled wild-type peptide to determine if this probe moiety affects binding. Full titration curves were not obtained, because sample amounts of the labeled peptides were limited.

## Electron paramagnetic resonance spectroscopy

X-band EPR spectra were obtained on a Varian E-109 spectrometer with a $TM_{102}$ cavity or a loop-gap resonator as described (Cherry, 1999). The microwave power was set at 1 mW with a field sweep of 160 G, a sweep time of 200 s, and an RF modulation of 1 G at 100 kHz. Spectra were obtained at 20–21°C. Peptides were in 5 mM phosphate buffer at pH 7.4 containing 150 mM NaCl (PBS).

Rotational correlation times for single Cys variant spin-labeled peptides were estimated by computer simulation, using the program developed by Freed and coworkers (Budil et al., 1996). Spectra were fitted to either a two- or three-component isotropic rotational diffusion model as judged by $\chi^2$ values. Input parameters to the fit include the known g tensor ($g_{xx}$ = 2.0086, $g_{yy}$ = 2.0066, $g_{zz}$ = 2.0032) and A tensor ($A_{xx}$ = 6.23, $A_{yy}$ = 6.23, $A_{zz}$ = 35.7) values for the MTSSL probe in an aqueous environment, as well as other well known physical parameters such as the nuclear gyromagnetic ratio, $\gamma$, and the nuclear spin, I. Parameters that are determined by the best fit simulation program are the rotational correlation time, $\tau_r$, and the fraction of each motional component, $f_r$. Thus, fitting of multicomponent spectra gave the relative population abundances and their associated $\tau_c$ values.

Other spectral parameters derived from the fit are the inhomogeneous line broadening and the phase. Neither of these parameters has any physical meaning in terms of spectrin structure, but both are the result of various spectroscopy artifacts. The inhomogeneous line broadening parameter is a function of probe properties, such as unresolved couplings to the methyl protons; and instrumental factors, chiefly of the spatial uniformity of the static magnetic field and the variation of this field by the RF modulation used by the phase sensitive detection system. Since we used 1 G modulation, this is a reasonable lower limit. Best fit values were typically in the range 1.0–1.3 G, and no significant differences in the motional parameters (e.g., $\tau_c$) were produced by fixing this parameter to $G_{mod}$ = 1 G. The phase was also allowed to vary to produce a best fit spectrum. Although the phase was routinely zeroed on a concentrated free spin label sample, small deviations from 0 (in all cases $<10^o$) in this parameter increased the goodness of fit as judged by $\chi^2$ values.

During fitting, a rotational model must be chosen. Many very sophisticated models may be chosen that may more fully describe the rotational diffusion operator; however, many of the more sophisticated models (Polimeno and Freed, 1995) require multi-frequency EPR at very high frequencies to be informative (Barnes et al., 1999). For simple X-band measurements, we are limited to less informative but more robust choices. The chief candidates are distinguished by their rotational symmetry group, i.e., whether the rotational diffusion tensor may be assumed to have spherical, axial, or rhombic symmetry. These choices yield, respectively, one ($\tau_{c\ mean}$), two ($\tau_{c\|}$ and $\tau_{c\perp}$), and three ($\tau_{cx}$, $\tau_{cy}$, and $\tau_{cz}$) rotational components. In the formalism of the fitting algorithm, these are related by the relationships $\tau_{c\ mean} = \sqrt[3]{(\tau_{c\|}\ \tau_{c\perp}^2)} = \sqrt[3]{(\tau_{cx}\ \tau_{cy}\ \tau_{cz})}$. The various models reveal progressively more information about the rotational properties of the molecule but also result in more uncertainties in the specific values of each parameter, which manifests itself in significant cross-correlations between these parameters (Budil et al., 1996). Conversely, more confidence can be ascribed to the simpler rotational model, which yields only a single mean $\tau_c$, the proviso being that the assumption of isotropic motion has been made, which may not exactly reflect the precise rotational properties of the probe. However, the mean value is still valid and has the advantage that it can be corroborated or refuted by other techniques that yield such quantitative values, such as our time-resolved fluorescence polarization (TRFP) experiments.

## Fluorescence polarization

TRFP experiments were performed at The Center for Dynamic Fluorescence at the University of Illinois (Urbana-Champaign, IL). The system and theory used for these measurements has been described (Jameson and Hazlett, 1991; Weber, 1977). Briefly, measurements were made by exciting with the 488-nm line of an Ar laser modulated at various frequencies (2–200 MHz) using a Pockels cell modulator. Probe lifetime data was first obtained by unpolarized excitation and an emission polarizer set at 55°. The lifetime of the probe was determined by simultaneously fitting the emission signal phase and modulation data appropriate equations, given in, e.g., Weber (1977) using the GLOBALS program (Beechem, 1992; Lakowicz et al., 1984; Jameson and Hazlett, 1991). Following this lifetime data acquisition, anisotropy decay measurements were taken on the same sample by using vertically polarized excitation and alternately with both parallel and than perpendicular emission polarizers. A range of modulation frequencies was again used to resolve fast and slow anisotropy decay components. Least-squares fitting to appropriate equations was conducted with the GLOBALS platform.

Analysis was again predicated on a rotational diffusion model. These are chiefly limited to how many components are resolved. In multicomponent models, these various components may or may not be assigned to parallel and perpendicular components. However, these simple fluorescence polarization measurements do not in general convey sufficient symmetry information (conveyed more readily in the EPR measurements in by the anisotropic A and g tensors) to make these assignments unambiguous. For this reason we have treated the $\tau_c$ values so obtained as $\tau_{c\ mean}$ for various as yet undefined components. This allows direct comparison to the EPR $\tau_{c\ mean}$ measurements, and so each may provide corroboration of the other.

# RESULTS

## Fidelity of the peptides

All the peptides produced exhibited substantially normal helicities, as measured by CD and compared to the wild-type peptide, as shown in Table 1. Values were within 7% of the wild-type value of 76% $\alpha$-helix. With the exception of the 28Cys and 49 Cys variants, all the singly Cys substituted peptides exhibited binding to $\beta$-spectrin. These $IC_{50}$ values were within 0.2 $\mu$M of the wild-type value of 0.3 $\mu$M (Cherry et al., 1999). The 28C and 49C variants did not appear to bind to $\beta$-spectrin. This result was not unexpected, as the presence of a Cys at the 28 position, or several other amino acids at the 49 position, has been previously shown to interfere with binding. In addition, conjugation of largest probe, fluorescein, was shown not to interfere with this binding. Displacements assays showed that the labeled pep-

**TABLE 1 Characterization of single Cys variant peptides**

| Labeling site | % helicity | $\beta$-spectrin binding ($\mu$M) |
|---|---|---|
| None (wt) | 76 | 0.3 |
| 14 | 76 | 0.4 |
| 21 | 71 | 0.5 |
| 28* | 70 | >20* |
| 35 | 69 | 0.4 |
| 42 | 76 | 0.4 |
| 49* | 76 | >20* |

Various measures of structural integrity were determined in order to ensure that these Cys substitutions did not unduly compromise the integrity of these proteins. It can be seen that all these variants are similar to the wild-type protein, with the exception that the 28C and 49C variants exhibited greatly reduced interaction with $\beta$-spectrin. This was expected, since these are known HE-causing mutations (*asterisks*).

tide displaced at least as much $^{125}$I-labeled wild-type peptide as the unlabeled precursor did. This indicated that the $IC_{50}$ values of the fluorescein labeled peptides were at least as low as the unlabeled precursors, which we showed above to be substantially similar to the wild-type peptide. Thus, we believe that these Cys substitutions did not unduly perturb the properties of the peptides studied.

## Probe motional properties

Rotational correlation times for the MTSSL spin probe were obtained from the EPR spectra (Cherry, 1999) of the singly labeled variant peptides by spectral simulation, Fig. 2. All spectra exhibited more than one component, which is the norm for this label coupled to a protein (Klug and Feix, 1998). Most positions were adequately simulated by utilizing a two-component model, with a fast and a slow $\tau_c$ population. In two cases (21Cys and 28Cys), an additional strongly immobilized component with $\tau_c \sim 80$ ns was observed, and is easily seen by eye in the $-1$ and $+1$ lines of the spectra of these variants (Fig. 2). This strongly immobilized component may be due to aggregation of the labeled peptides in solution. However, we could not remove this component by ultrafiltration or centrifugation, so macroscopic aggregates are not indicated. More likely, these spectral features represent a population of probes that are very strongly immobilized to the protein or are defects of our very simplified rotational model. Apparent motional parameters were determined for a minimum of three independent preparations of labeled peptides, and the mean values and standard errors are reported in Table 2.

Initial fluorescence experiments to obtain lifetime data showed that the decays were nearly bi-exponential, with a major long component (>90%) near 4.0 ns, and a minor

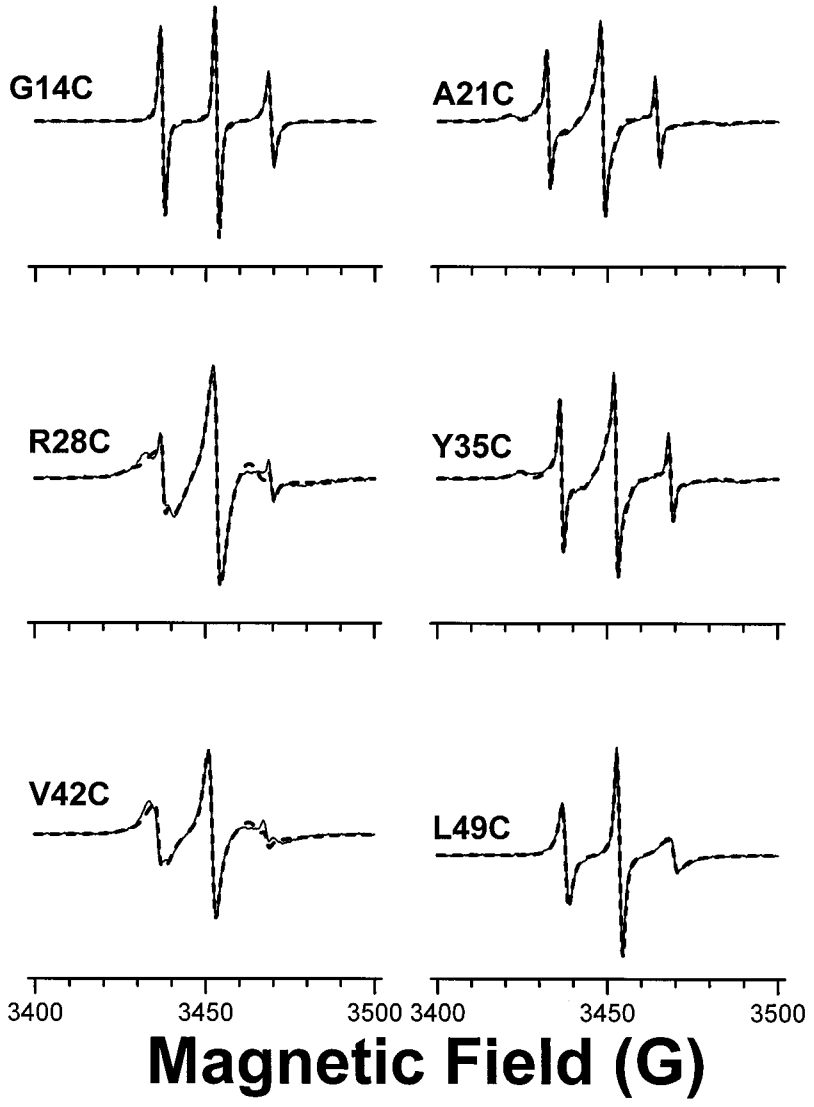


FIGURE 2 EPR spectra of the singly labeled peptides. Spectral simulation was used to obtain apparent rotational correlation times, according to the program developed by Freed and coworkers (Budil et al., 1996). These values can be seen in Table 2. Spectral simulation (*dashed lines*) was able to resolve two motional components from most of the experimental spectra (*solid lines*).

**TABLE 2 Motional parameters**

| Label position | EPR | | | | | | Fluorescence | | | |
|---|---|---|---|---|---|---|---|---|---|---|
| | $\tau_{c1}$ ns | f | $\tau_{c2}$ ns | f | $\tau_{c3}$ ns | f | $\tau_{c1}$ ns | f | $\tau_{c2}$ ns | f |
| 14 | 3.0 ± 0.4 | .22 | **7.1 ± 0.7** | .78 | n.d.* | | 0.2 ± 0.1 | .71 | **6.5 ± 0.6** | .29 |
| 21 | 1.4 ± 0.3 | .08 | **14.0 ± 1.6** | .45 | 74 ± 7 | .47 | 0.3 ± 0.2 | .53 | **13.7 ± 2.2** | .47 |
| 28 | 3.5 ± 1.5 | .06 | **19.5 ± 4.0** | .71 | 79 ± 20 | .22 | 0.3 ± 0.2 | .31 | **27.2 ± 1.9** | .69 |
| 35 | 1.9 ± 0.07 | .45 | **9.8 ± 1.8** | .55 | n.d.* | | 0.3 ± 0.2 | .50 | **12.8 ± 1.0** | .50 |
| 42 | 3.7 ± 0.6 | .09 | **17.0 ± 0.5** | .91 | n.d.* | | 0.2 ± 0.1 | .32 | **30.0 ± 3.5** | .68 |
| 49 | n.d. | | **10.0 ± 1.1** | 1.00 | n.d.* | | 0.3 ± 0.2 | .40 | **42.7 ± 0.2** | .60 |

*n.d.: none detected.

Motional components (mean values ± SE) and fractional signal intensity (f) for each labeled position for both EPR spectral simulation and TRFP measurements are shown, and are the result of 2 to 4 replicate measurements. For TRFP experiments, the data could be adequately simulated by a two-component model (no further reduction in $\chi^2$ could be achieved by implementing a third component). However, for certain samples, a third, strongly immobilized component was required to simulate the EPR spectra. In both cases, the fast component was ascribed to independent probe motion and is not of too great interest. Similarly, the slowest EPR component may be due to aggregated forms due to the higher concentration needed for EPR and is, again, of limited interest. We consider the intermediate component (in **bold type**) in both cases to be most relevant.

faster component $<1$ ns (data not shown). All peptides were similar, and similar to the value of 4.05 ns for free fluorescein in aqueous solution. TRFP experiments yielded differential phase and modulation data shown in Fig. 3. Fitting of this data to multicomponent rotational models by the GLOBALS program corroborated the presence of multiple components indicated by the EPR experiments. However, only two components were indicated by the experimental data. This may be due to the lower concentrations needed for the fluorescence experiments. The fast component produced by fitting the data was typically 0.2–0.3 ns. This value is poorly resolved, however, due to upper limits to the modulation frequency possible with the experimental setup, and typically had standard errors approaching the measure mean value. However, since this rapid motion is usually ascribed to independent probe motion, it has little bearing on the underlying peptide structure, and we did not devote additional effort to improving the accuracy of these points.

The slower motional component was, however, well within the modulation regime possible, and was accurately determined. Again, replicate determinations on separately prepared batches of peptides yielded mean values, and standard errors that are typically approximately 10% of this mean, as reported in Table 2.

## DISCUSSION

In order to understand the role of the amino terminal region of $\alpha$-spectrin in the spectrin tetramerization reaction, we have conducted certain experiments to probe the flexibility of this region. As previously discussed, it is thought, based on sequence homology and secondary structural algorithms, that this fractional motif interacts with a complementary fractional motif of the $\beta$-spectrin C-terminus to form a heteropolypeptide triple helical bundle. Based on this sequence homology, approximately residues 22–52 are homologous to an $\alpha$-helical structure, whereas residues 1–21 are atypical and appear to be unrelated to conserved repeat structures (Sahr et al., 1990), but have also been predicted to be $\alpha$-helical (Speicher et al., 1983a). It has also been proposed, based on protease cleavage data, that a helix begins at residue 17 and is separated from a smaller helix of approximately nine residues by a loop (Speicher et al., 1983b). However, predictive methods are imprecise and this region is not well understood.

This question has been addressed by making a series of mutant peptides which scan the $\alpha$-spectrin N-terminus and allow for spectroscopic probe attachment at specific residues along the N-terminus. The spin-label (MTSSL) and fluorescent label (5-IAF) were used as the spectroscopic probes coupled to the peptide at sequential "a" positions in the "abcdefg" heptad nomenclature for amphipathic $\alpha$-helices, and so should all be on the same face of the helix, if a helix exists. MTSSL has previously been shown to be one of the least structurally perturbing probes, and its short linker causes it to represent peptide mobility very faithfully (Hubbell et al., 1996; Mchaourab et al., 1996; Klug and Feix, 1998).

In coupling probes to protein structures, there is a concern that the structure of the protein is grossly disturbed and, therefore, not representative of the native structure. Thus, various studies were undertaken to ensure peptide stability and function. Gross structural integrity was assessed by determination of the peptide variants' helicity values, which are all very similar to the wild-type peptide; however, the observed signal should be dominated by the helices of the three structural domains (residues 52–368), so it is difficult to detect accurately any small deviations that might occur. Thus, to examine just the N-terminal region and to examine the functionality of these peptides, the binding of the single Cys variants to $\beta$-spectrin was examined. Most of the single Cys variants exhibit binding to $\beta$-spectrin with affinities in the 0.3- to 0.5-$\mu$M range, except for the 28C and 49C variants. The 28C variant is a clinically observed hereditary

anemia-causing mutation that is known to impair spectrin association (Coetzer et al., 1991), so this non-binding behavior was not unexpected. The non-binding behavior ($IC_{50} > 20\ \mu M$) for the 49C mutant is also not unexpected, since although the specific Cys substitution has not been observed, other amino acid substitutions here can cause hereditary anemias (Garbarz et al., 1990; Morle et al., 1990). Since this variant does exhibit helicity identical to the wild-type peptide, the overall structure of the peptide is probably not deleteriously disturbed. We have also recently determined that the entirety of this region exhibits $\alpha$-helical signals in double spin-labeling studies (Cherry et al., 2000). It should also be noted that since the amino-terminal region of $\alpha$-spectrin is known to contain a large majority of mutations resulting in impaired tetramerization, it is extremely difficult to scan this region systematically without encountering sensitive mutation positions. Single point displacement assays show that probe attachment to these Cys variants does not appear to interfere with binding.

EPR spectral line shapes were analyzed by spectral simulation to provide motional information about the attached probe. In all cases several motional components were observed; this phenomenon is well known to be the rule rather that the exception with this spin probe coupled to proteins (Klug and Feix, 1998). This multicomponent behavior poses a problem for other methods of motional analysis from EPR line shapes such as line width ($\Delta H^0$) or second moment ($<H2>$) methods (Hubbell et al., 1998; Mchaourab et al., 1996), because the spectra will be dominated by the sharper rapid components. It is also unclear how such EPR-specific parameters can be directly compared with other techniques that measure mobility, such as our TRFP measurements. For this reason we pursued spectral simulation to attempt to resolve these various components, so that we could determine them independently.

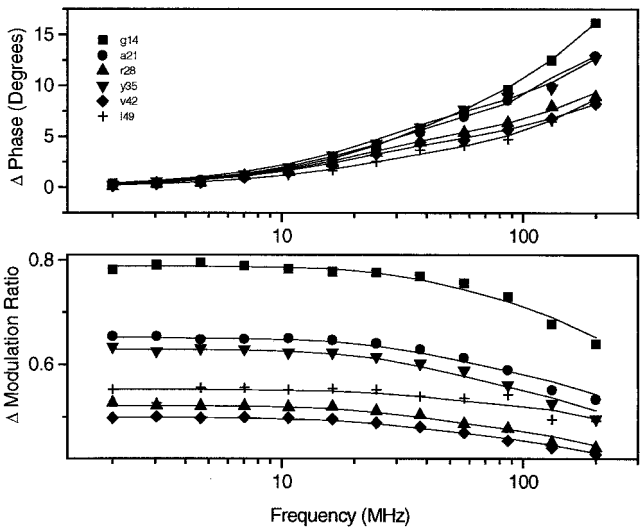


FIGURE 3 TRFP phase and modulation mobility data. Representative phase and modulation data are shown. For peptides with a slow rotational time, the differential phase peak shifts to lower frequencies and the peak amplitude decreases. Increasing rotational times can also be seen from the modulation data as reduced modulation ratios at low frequencies. The rotational correlation times are listed in Table 2. The *top graph* shows the phase data. The *bottom graph* shows the modulation data.

However, this approach, though more rigorous, does involve separate problems. Firstly, the spectra are sensitive not only to the rotational rate, but also to the peculiarities of the nature of the rotational diffusion operator. It has recently been shown that the motion of spin probes on polypeptides is very complex, and that multi-frequency experiments may be necessary to fully describe the motion (Barnes et al., 1999). In that work, it was shown that examination of the X-band data alone with simple rotational models can yield values that are an admixture of backbone and overall peptide motion, but that these components can be separated by inclusion of very high frequency data, which effectively freezes out the slower motions. However, the separation into local and global motions is itself a gross oversimplification, as a full examination of the flexibility of a macromolecule involves hundreds of motional modes which will be detected in the probe spectra to varying degrees (Go, 1990). As such, we and others (Langen et al., 1999; Owenius et al., 1999) have sought only to determine an apparent flexibility from the X-band data alone, while acknowledging the approximations in this approach. In this study, we used a spherical model, which yields only a single parameter for each component to describe the rotational diffusion of the molecule. This sacrifices accuracy of the simulation, in the hope that the average $\tau_c$ value so determined will be more robust.

The second problem when considering this spectral simulation method is how to interpret the various components. Methods that yields only a single proxy for motion, i.e., $\Delta W0$ or $<H2>$, ignore this problem, because all the components are averaged (but usually in some unknown way) into this single parameter. In our case, spectral simulation has resolved at least two components. The fastest component, in the low nanosecond range, is typically assigned to independent probe motion, and is not usually of great interest, in that it does not inform us about the underlying peptide motion. However, the correlation times of 1–3 ns are higher than that for free probe in solution (<1 ns), and so some restriction of motion is indicated. It has recently been demonstrated by NMR (d'Avignon et al., 1998; Holtzer et al., 1997) and FTIR (Venyaminov et al., 1999) techniques that helical peptides can exist in an equilibrium between disordered and helical states in solution, and that this equilibrium varies between individual positions in the same peptide. The disordered population in this interpretation may be similar to the fast $\tau_c$ population in this study.

The second motional component with longer $\tau_c$, in our case 6–40 ns, is in the appropriate range for a peptide motion for the spectrin fragment studied here (~45 kDa). We have assigned this component to backbone motion of the peptide. This is not the same as overall motion of the

peptide as a whole, but rather reflects the degree to which the particular labeling position couples to the rest of the peptide. Similar interpretations have been made in other helical peptides (Miick et al., 1991; Todd and Millhauser, 1991) in which the model free order parameter S was calculated to quantify this coupling. In other formalisms, this component may be seen to be homologous the $\tau_{c\ backbone}$ of Hubbell (Mchaourab et al., 1996).

Two peptides exhibited spectra that yielded a third motional component, with a much longer apparent $\tau_c$, ~80 ns. This minor, strongly immobilized component is commonly seen with protein spin-labeled with the MTSSL probe. There are various possible explanations for this component. The simplest assignment is to oligomers of the parent peptide. Such oligomers have been previously observed for a related, slightly longer, version of this spectrin fragment by light scattering techniques. This component could not be removed by filtration, or lower speed ($13000 \times g$) centrifugation, and so does not appear to be the result of macroscopic aggregates. Alternatively, this component may represent very strongly immobilized probe species, involving interactions of the nitroxide ring structure with the rest of the protein molecule. The conventional view is that, normally, the MTSSL probe has a linker arm strongly tethered by hydrogen bonding to the disulfide moiety, but that the ring moiety is relatively free to rotate about the $C^{\epsilon}$-$S^{\delta}$ bond, and so can partially average the A and g tensors. In some cases it appears that an anomalous interaction may occur with the ring system and the protein, further immobilizing at least a portion of the labels, and resulting in a component exhibiting very anisotropic hyperfine interactions (Mchaourab et al., 1999). The extent of this undesirable interaction seems to be somewhat idiosyncratic. In any event, such behavior has little bearing on the local secondary structure at the coupling site, the immediate object of this study, so we will not be concerned with it further.

Because of the various ambiguities expressed above in the interpretation of the EPR data, we sought an independent corroboration of these values to make our interpretation more convincing. This took the form of TRFP experiments, which also yield information about the rotational diffusion of probes attached to identical positions on the molecule. Again, multicomponent behavior was observed, with fast and slow components evident. In this case, the fast components were $<1$ ns, and so were confidently assigned to independent probe motion. Many similar fluorescent probes often exhibit such residual motion when coupled to the surface of proteins. The slower $\tau_c$ time was again assigned to backbone motion. In no case was a third, very slow component observed. This may be due to the actual absence of oligomers due to the lower concentrations required for fluorescence experiments, but it also may be due to the relatively short lifetimes (in all cases ~4 ns) of the probe used, which precluded observation in this range.

The agreement of $\tau_{c\ 2\ EPR}$ and $\tau_{c\ 2\ fl}$ was very good, as tabulated in Table 2 and shown in Fig. 4 *A*. It is notable that the correlation is not good for $\tau_{c\ 1}$, which we have assigned to independent probe motion and so is a property of the different probes used for the two techniques. In contrast, the $\tau_{c\ 2}$ times have been assigned to backbone motion, and thus should be a property of the peptide, not the probe, which is of course identical in each case. For the 14, 21, 28, and 35 positions the agreement is very good and the error bars overlap or nearly overlap. At the 42 position there is some disagreement, and at the 49 position this disagreement is much larger. It is possible that the 5IAF probe is interacting significantly with the first complete triple $\alpha$-helical bundle (immediately adjacent to these positions at residues 52–156) and so reporting on the motion of this larger more rigid domain. 5IAF is larger, more hydrophobic, and has a longer linker region than MTSSL and so such behavior is not unexpected. However, the overall patterns of $\tau_c$ at each position, by both techniques, are remarkably similar. The amounts of fast component, which may reflect the local equilibrium between helical and unwound (random or disor-

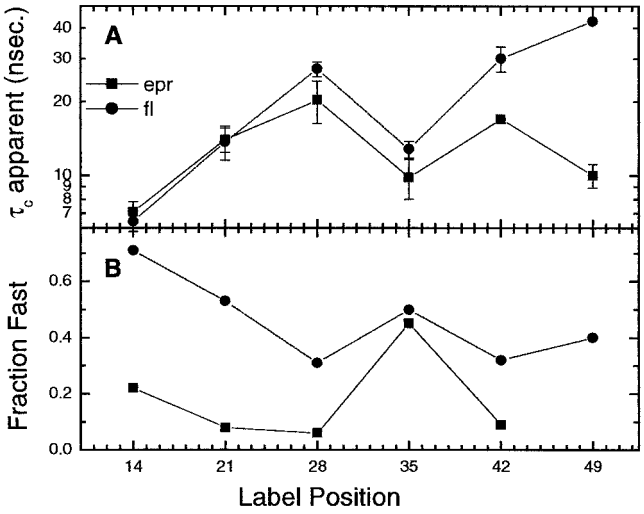


FIGURE 4 Comparison of EPR and fluorescence flexibilities. EPR (*squares*) and TRFP (*circles*) data are compared at all the positions studies. Mean values, with error bars representing standard error of mean, are shown. (*A*) Apparent $\tau_{r\ slow}$ versus probe position are plotted. The two techniques give similar results, overlapping at most positions, suggesting that these measurements reflect an underlying property of the spectrin molecule and not an artifact of the spectroscopic technique or analysis model. The discrepancy at later positions (especially 49) may be due the larger and more hydrophobic nature of the fluorescent probe compared to the paramagnetic probe, as discussed in more detail in the text. (*B*) The percentages of $\tau_{r\ fast}$ (defined as $<10$ ns) versus probe position are plotted. It can be seen that a larger fast component occurs in the TRFP than in the EPR experiments. This is a well known problem for these types of fluorophore couplings, in which a large fraction of the motion is observed to be independent probe motion, especially when the probe molecule is coupled to the surface of a protein. In any case, it can be seen that the two measurements show a similar relative pattern, with the fractional fast component in general decreasing toward the C-terminus of the region, and a similar anomaly occurring at position 35.

dered) structures also show similar trends between positions, Fig. 4 *B*, although the MTSSL probe shows much less of this fast component in general than the 5IAF probe. This is not surprising, since we specifically used the MTSSL probe to take advantage of its very tight coupling to protein structures. These agreements increase our confidence that we are actually reporting on local peptide flexibility, and not some artifact of the spectroscopic technique or the models used to interpret the spectra.

In general, these slow rotational correlation times shows that as the probe approaches the first structural domain (residue 52; Lusitani et al., 1994) there is an increase in $\tau_c$, indicating tighter coupling to the molecule as a whole, and thus the presence of some structure. This increase is consistent from 14 to 49, with the exception of position 35 which will be discussed later. Position 14, which is outside the region shown to be essential for $\beta$-spectrin binding, is not as tightly coupled to the rest of the molecule as seen from the rotational correlation time of $\sim$7 ns. The beginning of some structure seems likely from position 21 onward.

The varying times reported by probes at each position reflect the varying degree to which each position is coupled to the rest of the molecule. Long times, (i.e., rigid regions) do not, in and of themselves, imply structure or order. However, we have previously shown that all of these regions do show signals strongly suggestive of an $\alpha$-helix by double label coupling experiments (Cherry et al., 2000). That study, however, showed that the extent to which this signal was seen at each position was variable, implying that some of these regions are "more helical" than others. The dynamic data in this study provides and explanation for this observation: the helix appears to unwind at equilibrium to varying extents along its length. This dynamic behavior may have important biological implications, since we have demonstrated (Cherry et al., 1999) that the spectrin tetramer association must be the driven by something other than simply the association of the this(putatively helical) region with its complimentary region in $\beta$-spectrin. The freezing out of this disorder to form a more fully helical structure may provide this extra impetus.

Position 35 shows increased mobility in the region of structured order. Many secondary prediction algorithms predict a break in the helix at or near this point, e.g., the SSP protocol (Salamov and Solovyev, 1997) or the NNPREDICT (Kneller et al., 1990). Because both experimental methods showed increased flexibility and the predictive methods indicate some helical disruption at this point, it seems likely that there may be some structural disturbance at this point. However, we cannot rule out the possibility that the mutagenesis of residue 35 to Cys has disrupted a previously well folded, helical region in the wild-type molecule. Cys is typically considered to have moderate helical propensity, greater in fact than the Tyr that it replaces in the wild-type molecule. Recently it has been demonstrated that when the Cys is conjugated to the MTSSL paramagnetic probe, the Cys-probe moiety has even greater helical propensity (Bolin et al., 1998). These two factors conspire to imply that the anomalously high mobility seen here is unlikely to be an artifact of the probe coupling technology; however, further higher resolution studies are needed.

These results may be compared to a previously suggested schematic representation of this region based on secondary structural algorithms (Speicher et al., 1993). There is agreement with the major helical region residing approximately between residues 20–52. This is in contrast to studies on isolated 1–53 peptide, which showed no secondary structure. However, as we have previously demonstrated, substantial structural cooperativity exists between adjacent triple $\alpha$-helical bundle motifs (Menhart et al., 1996; Lusitani et al., 1998), which raises the possibility that the stability of the region may be enhanced when in tandem with the subsequent more stable complete structural domains. We have shown herein that this region exhibits rigidity incompatible with a disordered structure, so that is seems likely that this region is in fact helical even in the absence of association with $\beta$-spectrin.

This work was supported by the American Heart Association (Grant-in-aid 9708064A to N. M.). L. C. was supported by a Graduate Assistance in Areas of National Need (GAANN) Fellowship. We are also very grateful for the use of equipment at the Laboratory for Fluorescence Dynamics at the University of Illinois at Champaign-Urbana, a National Institutes of Health supported center. LWMF was supported by an NSF grant (#MLB 98 01870).

## REFERENCES

Agre, P. 1992. Clinical relevance of basic research on red cell membranes. *Clin. Res.* 40:176–186.

Barnes, J. P., Z. Liang, H. S. Mchaourab, J. H. Freed, and W. L. Hubbell. 1999. A multifrequency electron spin resonance study of T4 lysozyme dynamics. *Biophys. J.* 76:3298–3306.

Beechem, J. M. 1992. Global analysis of biochemical and biophysical data. *Methods Enzymol.* 210:37–54.

Begg, G. E., M. B. Morris, and G. B. Ralston. 1997. Comparison of the salt-dependent self-association of brain and erythroid spectrin. *Biochemistry.* 36:6977–6985.

Begg, G. E., G. B. Ralston, and M. B. Morris. 1994. A proton nuclear magnetic resonance study of the mobile regions of human erythroid spectrin. *Biophys. Chem.* 52:63–73.

Bolin, K. A., P. Hanson, S. J. Wright, and G. L. Millhauser. 1998. An NMR investigation of the conformational effect of nitroxide spin labels on Ala-rich helical peptides. *J. Magn. Reson.* 131:248–253.

Budil, D. E., S. Lee, S. Saxena, and J. H. Freed. 1996. Nonlinear-least-squares analysis of slow motion EPR spectra in one and two dimension using a modified Levenberg-Marquardt algorithm. *J. Magn. Reson. Series A* 120:155–189.

Byers, T. J., and D. Branton. 1985. Visualization of the protein associations in the erythrocyte membrane skeleton. *Proc. Natl. Acad. Sci. USA.* 82:6153–6157.

Cherry, L. 1999. Binding and structural studies of the a-spectrin N-terminus. Ph.D. thesis in the Department of Chemistry, Loyola University of Chicago (Chicago, IL).

Cherry, L., N. Menhart, and L. W. Fung. 1999. Interactions of the alpha-spectrin N-terminal region with beta- spectrin. Implications for the spectrin tetramerization reaction. *J. Biol. Chem.* 274:2077–2084.

Cherry, L., N. Menhart, and L. W.-M. Fung. 2000. Spin-label EPR structural studies of the N-terminus of α-spectrin. *FEBS Letts.* 466:341–345.

Coetzer, T. L., K. Sahr, J. Prchal, H. Blacklock, L. Peterson, R. Koler, J. Doyle, J. Manaster, and J. Palek. 1991. Four different mutations in codon 28 of alpha spectrin are associated with structurally and functionally abnormal spectrin alpha I/74 in hereditary elliptocytosis. *J. Clin. Invest.* 88:743–749.

d'Avignon, D. A., G. L. Bretthorst, M. E. Holtzer, and A. Holtzer. 1998. Site-specific thermodynamics and kinetics of a coiled-coil transition by spin inversion transfer NMR. *Biophys. J.* 74:3190–3197.

DeSilva, T. M., K. C. Peng, K. D. Speicher, and D. W. Speicher. 1992. Analysis of human red cell spectrin tetramer (head-to-head) assembly using complementary univalent peptides. *Biochemistry.* 31: 10872–10878.

Eber, S. W., S. A. Morris, W. Schroter, and W. B. Gratzer. 1988. Interactions of spectrin in hereditary elliptocytes containing truncated spectrin beta-chains. *J. Clin. Invest.* 81:523–530.

Gallagher, P. G., W. T. Tse, S. L. Marchesi, H. S. Zarkowsky, and B. G. Forget. 1991. A defect in alpha-spectrin mRNA accumulation in hereditary pyropoikilocytosis. *Trans. Assoc. Am. Physicians.* 104:32–39.

Garbarz, M., M. C. Lecomte, C. Feo, I. Devaux, C. Picat, C. Lefebvre, F. Galibert, H. Gautero, O. Bournier, C. Galand, B. G. Forget, P. Boivin, and D. Dhermy. 1990. Hereditary pyropoikilocytosis and elliptocytosis in a white French family with the spectrin alpha I/74 variant related to a CGT to CAT codon change (Arg to His) at position 22 of the spectrin alpha I domain. *Blood.* 75:1691–1698.

Go, N. 1990. A theorem on amplitudes of thermal atomic fluctuations in large molecules assuming specific conformations calculated by normal mode analysis. *Biophys. Chem.* 35:105–112.

Grum, V. L., D. Li, R. I. MacDonald, and A. Mondragon. 1999. Structures of two repeats of spectrin suggest models of flexibility. *Cell.* 98:523–35.

Holtzer, M. E., E. G. Lovett, D. A. d'Avignon, and A. Holtzer. 1997. Thermal unfolding in a GCN4-like leucine zipper: 13C alpha NMR chemical shifts and local unfolding curves. *Biophys. J.* 73:1031–1041.

Hubbell, W. L., A. Gross, R. Langen, and M. A. Lietzow. 1998. Recent advances in site-directed spin labeling of proteins. *Curr. Opin. Struct. Biol.* 8:649–656.

Hubbell, W. L., H. S. McHaourab, C. Altenbach, and M. A. Lietzow. 1996. Watching proteins move using site-directed spin labeling. *Structure.* 4:779–783.

Jameson, D. M., and T. L. Hazlett. 1991. Time resolved fluorescence in biology and biochemistry. *In* Biophysical and Biochemical Aspects of Fluorescence Spectroscopy. Dewey, G. T., ed. Plenum Press, New York. 294.

Klug, C. S., and J. B. Feix. 1998. Site-directed spin labeling of membrane proteins and peptide-membrane interactions. *In* Biological Magnetic Resonance: Spin labeling: The Next Millennium, vol. 14. Berliner, L. J., ed. Plenum Press, New York. 251–281.

Kneller, D. G., F. E. Cohen, and R. Langridge. 1990. Improvements in protein secondary structure prediction by an enhanced neural network. *J. Mol. Biol.* 214:171–182.

Lakowicz, J. R., E. Gratton, H. Cherek, B. P. Maliwal, and G. Laczko. 1984. Determination of time-resolved fluorescence emission spectra and anisotropies of a fluorophore-protein complex using frequency-domain phase-modulation fluorometry. *J. Biol. Chem.* 259:10967–10972.

Langen, R., K. Cai, C. Altenbach, H. G. Khorana, and W. L. Hubbell. 1999. Structural features of the C-terminal domain of bovine rhodopsin: a site-directed spin-labeling study. *Biochemistry.* 38:7918–7924.

Liu, S. C., L. H. Derick, and J. Palek. 1987. Visualization of the hexagonal lattice in the erythrocyte membrane skeleton. *J. Cell Biol.* 104:527–536.

Lusitani, D., N. Menhart, T. A. Keiderling, and L. W. Fung. 1998. Ionic strength effect on the thermal unfolding of alpha-spectrin peptides. *Biochemistry.* 37:16546–16554.

Lusitani, D. M., N. Qtaishat, C. C. LaBrake, R. N. Yu, J. Davis, M. R. Kelley, and L. W. Fung. 1994. The first human alpha-spectrin structural domain begins with serine. *J. Biol. Chem.* 269:25955–25958.

Marchesi, S. L. 1989. Red Blood Cell Membranes: Structure, Function, and Clinical Implications. Marcel Dekker, Inc., New York.

McGuire, M., and P. Agre. 1988. Clinical disorders of the erythrocyte membrane skeleton. *Hematol. Pathol.* 2:1–14.

Mchaourab, H. S., T. Kalai, K. Hideg, and W. L. Hubbell. 1999. Motion of spin-labeled side chains in T4 lysozyme: effect of side chain structure. *Biochemistry.* 38:2947–2955.

Mchaourab, H. S., M. A. Lietzow, K. Hideg, and W. L. Hubbell. 1996. Motion of spin-labeled side chains in T4 lysozyme: Correlation with protein structure and dynamics. *Biochemistry.* 35:7692–7704.

Menhart, N., T. Mitchell, D. Lusitani, N. Topouzian, and L. W. Fung. 1996. Peptides with more than one 106-amino acid sequence motif are needed to mimic the structural stability of spectrin. *J. Biol. Chem.* 271:30410–30416.

Miick, S. M., A. P. Todd, and G. L. Millhauser. 1991. Position-dependent local motions in spin-labeled analogues of a short alpha-helical peptide determined by electron spin resonance. *Biochemistry.* 30:9498–9503.

Morle, L., A. F. Roux, N. Alloisio, B. Pothier, J. Starck, L. Denoroy, F. Morle, R. C. Rudigoz, B. G. Forget, and J. Delaunay. 1990. Two elliptocytogenic alpha I/74 variants of the spectrin alpha I domain. Spectrin Culoz (GGT—-GTT; alpha I 40 Gly—-Val) and spectrin Lyon (CTT—-TTT; alpha I 43 Leu—Phe). *J. Clin. Invest.* 86:548–554.

Morris, M., and G. B. Ralston. 1989. A thermodynamic model for the self-association of human spectrin. *Biochemistry.* 28:8561–8567.

Morris, M. B., and G. B. Ralston. 1994. Biophysical characterization of membrane and cytoskeletal proteins by sedimentation analysis. *Subcell. Biochem.* 23:25–82.

Owenius, R., M. Osterlund, M. Lindgren, M. Svensson, O. H. Olsen, E. Persson, P. O. Freskgard, and U. Carlsson. 1999. Properties of spin and fluorescent labels at a receptor-ligand interface. *Biophys. J.* 77:2237–2250.

Palek, J., and S. Lambert. 1990. Genetics of the red cell membrane skeleton. *Semin. Hematol.* 27:290–332.

Pascual, J., M. Pfuhl, D. Walther, M. Saraste, and M. Nilges. 1997. Solution structure of the spectrin repeat: a left-handed antiparallel triple-helical coiled-coil. *J. Mol. Biol.* 273:740–751.

Polimeno, A., and J. H. Freed. 1995. Slow Motional Esr in Complex Fluids-the Slowly Relaxing Local Structure Model of Solvent Cage Effects. *J. Phys. Chem.* 99:10995–11006.

Sahr, K. E., P. Laurila, L. Kotula, A. L. Scarpa, E. Coupal, T. L. Leto, A. J. Linnenbach, J. C. Winkelmann, D. W. Speicher, V. T. Marchesi, P. Curtis, and B. G. Forget. 1990. The complete cDNA and polypeptide sequences of human erythroid alpha- spectrin. *J. Biol. Chem.* 265: 4434–4443.

Salamov, A. A., and V. V. Solovyev. 1997. Protein secondary structure prediction using local alignments. *J. Mol. Biol.* 268:31–36.

Shotton, D. M., B. E. Burke, and D. Branton. 1979. The molecular structure of human erythrocyte spectrin. Biophysical and electron microscopic studies. *J. Mol. Biol.* 131:303–329.

Speicher, D. W., G. Davis, and V. T. Marchesi. 1983a. Structure of human erythrocyte spectrin. II. The sequence of the alpha- I domain. *J. Biol. Chem.* 258:14938–14947.

Speicher, D. W., G. Davis, P. D. Yurchenco, and V. T. Marchesi. 1983b. Structure of human erythrocyte spectrin. I. Isolation of the alpha-I domain and its cyanogen bromide peptides. *J. Biol. Chem.* 258:14931–14937.

Speicher, D. W., T. M. DeSilva, K. D. Speicher, J. A. Ursitti, P. Hembach, and L. Weglarz. 1993. Location of the human red cell spectrin tetramer binding site and detection of a related "closed" hairpin loop dimer using proteolytic footprinting. *J. Biol. Chem.* 268:4227–4235.

Speicher, D. W., J. S. Morrow, W. J. Knowles, and V. T. Marchesi. 1982. A structural model of human erythrocyte spectrin: alignment of chemical and functional domains. *J. Biol. Chem.* 257:9093–9101.

Speicher, D. W., L. Weglarz, and T. M. DeSilva. 1992. Properties of human red cell spectrin heterodimer (side-to-side) assembly and identification of an essential nucleation site. *J. Biol. Chem.* 267:14775–14782.

Todd, A. P., and G. L. Millhauser. 1991. ESR spectra reflect local and global mobility in a short spin-labeled peptide throughout the alpha-helix—coil transition. *Biochemistry.* 30:5515–5523.

Venyaminov, S. Y., Hedstrom, J. F., and F. G., P. 1999. Analysis of the segmental stability of helical peptides by isotope-edited infrared spectroscopy. *Protein Sci.* 8: 241-S.

Vertessy, B. G., and T. L. Steck. 1989. Elasticity of the human red cell membrane skeleton: effects of temperature and denaturants. *Biophys. J.* 55:255–262.

Weber, G. 1977. Theory of differential phase fluorometry: detection of anisotropic molecular rotations. *J. Chem. Phys.* 66:4081–4091.

Winkelmann, J. C., J. G. Chang, W. T. Tse, A. L. Scarpa, V. T. Marchesi, and B. G. Forget. 1990. Full-length sequence of the cDNA for human erythroid beta-spectrin. *J. Biol. Chem.* 265:11827–11832.

Yan, Y., E. Winograd, A. Viel, T. Cronin, S. C. Harrison, and D. Branton. 1993. Crystal structure of the repetitive segments of spectrin. *Science.* 262:2027–2030.